JOURNAL OF MATERIALS SCIENCE 26 (1991) 889–898

Dual ferrite–martensite treatments of a high-strength low-alloy ASTM A588 steel

J. R. YANG
Institute of Materials Engineering, National Taiwan University, Taipei, Taiwan
L. J. CHEN
Department of Materials Science and Engineering, National Tsing Hua University, Hsinchu, Taiwan

Dual ferrite–martensite (DFM) treatments of an ASTM A588 steel have been investigated. The treatments consisted of initial austenitization and quenching to form 100% martensite, followed by annealing in the $(\alpha + \gamma)$ region and subsequent quenching. It was found that DFM microstructures of the steel contained continuous globular martensite along the prior austenite grain boundaries and acicular martensite within the prior austenite grains. The DFM of the steel exhibited the superb combinations of strength and elongation over a range of elongation 15% to 20% in a 3 cm gauge length. For a sample with 18% elongation, the yield strength was 49 kg mm^{-2} (70×10^3 p.s.i.) and the ultimate tensile strength 68 kg mm^{-2} (97×10^3 p.s.i.). The type of initial microstructure prior to the dual phase treatment is of prime importance in the determination of the morphology of DFM structure. The results show that the initial martensite structure is more advantageous than the initial pearlite plus proeutectoid ferrite and austenite structures.

1. Introduction

Dual ferrite–martensite (DFM) steels have received a great deal of attention in the past for improved strength and weight applications [1–8], because they contain characteristic microstructural features that combine high strength with good formability. These two-phase steels contain controlled amounts of martensite (strong phase) in a ferrite matrix (soft phase), and are capable of optimizing the ever conflicting property requirements of strength and ductility, dependent upon a favourable choice of alloy composition and processing. This composite system is of interest because the required microstructures can be produced simply by utilizing solid-state phase transformations without resorting to mechanical or thermomechanical treatments.

ASTM A588 steel is one of the most widely used classes of high-strength low-alloy (HSLA) steels. HSLA steels are a group of steels intended for general structural or miscellaneous applications and that have specified minimum yield points above about 28 kg mm^{-2} (40×10^3 p.s.i.). These steels typically contain small amounts of alloying elements to achieve their strength in the hot-rolled or normalized condition. The principal strengthening of these HSLA steels is derived from precipitation of finely dispersed alloy carbides and grain refinement [9].

ASTM A588 steel possesses the property of atmospheric-corrosion resistance, so it may be employed to weight-saving applications by utilizing thinner steel plates in service. It is desirable to understand the relationship between the DFM structures of the steel and the mechanical properties. By investigation of the detailed relationship between microstructures and properties, a simple, economical heat treatment may be found to obtain optimum mechanical properties of the steel for industrial processing.

In this study, the heat treatment consists of initial austenitization and quenching to form 100% martensite, followed by annealing in the $(\alpha + \gamma)$ region and subsequent quenching. The austenitization was performed at 1100 °C for 30 min. The principal reason for these choices is to dissolve all carbide [3]. The annealing temperatures in the $(\alpha + \gamma)$ region were chosen as 825, 800, 775 and 750 °C as shown in Fig. 1a; this equilibrium diagram was derived from the data presented by Bain and Paxton [10] and is applicable for alloys containing 1 to 2 wt % Mn.

2. Experimental procedure

ASTM A588 steel samples were received as hot-rolled bars. The compositions of the steel are listed in Table I. The thickness of the bars was 3.5 cm. The bars were forged at 1000 to 1100 °C into 3 and 12 mm thick plates. Homogenization treatment was done at 1100 °C for 2 h in an air furnace, then the specimens were air-cooled. To minimize decarburization and oxidation, the specimens were enclosed in a stainless steel box and covered with the baked refractory powder.

0022–2461/91 $03.00 + .12

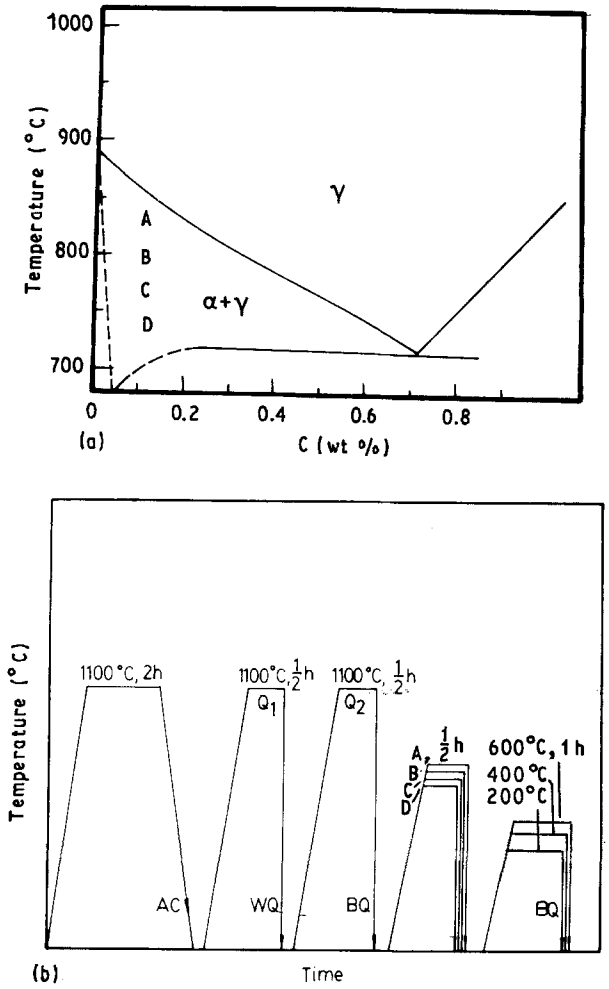

Figure 1 (a) Phase diagram of the Fe–1 wt % Mn–C model steel. (b) Schematic diagram of the heat treatments. A, 825 °C; B, 800 °C; C, 775 °C; D, 750 °C.

A set of samples for tensile testing, optical microscopy and transmission electron microscopy were prepared from the 3 mm thick plates. Charpy impact test specimens were obtained from the 12 mm thick plates.

After being austenitized in an inert argon atmosphere at 1100 °C for 30 min, the specimens were quenched directly into water (Q_1 treatment). For a high quenching rate, all the specimens were austenitized in a salt bath kept at 1100 °C for 30 min and quenched directly into brine (Q_2 treatment).

For two-phase annealing, samples were immersed in the salt bath at 825, 800, 775 and 750 °C, for 30 min, then quenched directly into brine. The samples for tensile and Charpy test were labelled A30, B30, C30 and D30 etc., where the letters A, B, C and D refer to annealing temperatures of 825, 800, 775 and 750 °C, respectively, and the digits represent the annealing time in minutes. For example, A30 represents a sample annealed at 825 °C for 30 min. Tempering of A30, B30, C30 and D30 samples was performed in a salt bath kept at the desired temperatures, e.g. 200, 400 and 600 °C, for 1 h. The detailed heat-treatment schemes are given in Fig. 1b. To avoid the effect of decarburization, the exposed surfaces of the tensile test and Charpy impact test specimens were ground away.

The type of initial microstructure prior to DFM treatment is of prime importance in the determination of the morphology of DFM structure. Three different heat-treatment processes (Fig. 2) were used to study the mechanical properties of specific DFM structure and the effect of initial structure prior to subsequent annealing in the ($\alpha + \gamma$) region.

1. Process I: the homogenized samples were immersed in the high-temperature salt bath kept at 1100 °C for 30 min and quenched directly into ice–brine. For two-phase annealing, the samples were immersed in a salt bath at either 800, 775 or 750 °C, for 20 min, then quenched directly into ice–brine.

2. Process II: the homogenized samples, with proeutectoid ferrite plus fine perlite structure, were immersed in a salt bath kept at either 800, 775 or 750 °C, for 20 min, then quenched directly into ice–brine.

3. Process III: the homogenized samples were immersed in the high-temperature salt bath kept at 1100 °C for 30 min and quenched directly into another salt bath kept at either 800, 775 or 750 °C, for 20 min, then quenched directly into ice–brine.

The grain size of the prior austenite detected in the full martensite sample and the volume fraction of martensite in DFM were examined by optical metallography. Ultimate tensile strength (UTS), yield strength (YS) and elongation of the sample were measured with an Instron tensile machine Model 1115. The hardness values were obtained with a Rockwell hardness tester with a C scale (RC). Microstructures and fractography were studied in order to determine the microstructure–mechanical property relationship with optical microscopy (OM), transmission and scanning electron microscopy (TEM, SEM). The Charpy impact energy and the ductile to brittle transition temperature (DBTT) were measured with a Charpy impact tester with a 30 kg m capacity.

3. Results

3.1. Dual-phase-treated samples

3.1.1. Mechanical properties

3.1.1.1. Tensile properties. The tensile properties of dual-phase-treated samples are shown in Figs 3 to 7 for hardness, strength and elongation versus volume fraction of martensite and strength versus elongation, respectively.

Fig. 3 shows the variation of the Rockwell hardness on a C scale of two-phase annealed specimens as a function of volume fraction of martensite. It shows that the hardness increases linearly with volume fraction of martensite.

TABLE I Compositions of the steel (wt %)

C	Mn	Cr	Si	Cu	V	Al	Ni	S	P	Mo
0.16	1.24	0.54	0.27	0.27	0.045	0.040	0.020	0.014	0.013	0.010

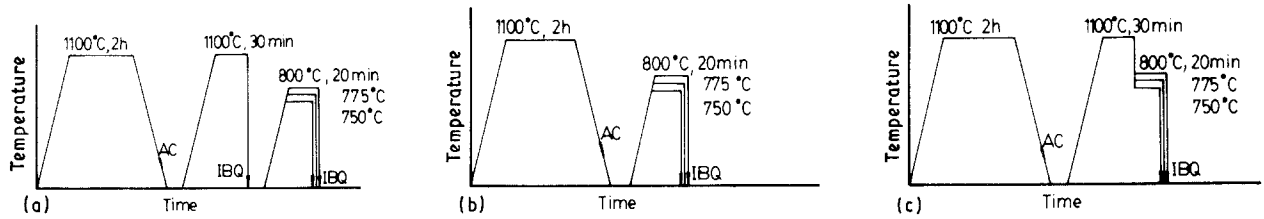

Figure 2 (a) to (c) The three heat-treatment schemes (I to III, respectively) to produce different initial microstructures.

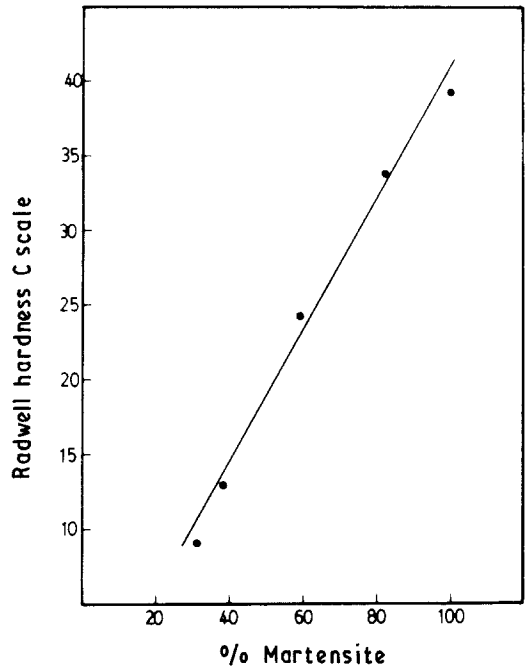

Figure 3 The variation of hardness of Q_2 and dual-phase treated specimens with the volume fraction of martensite.

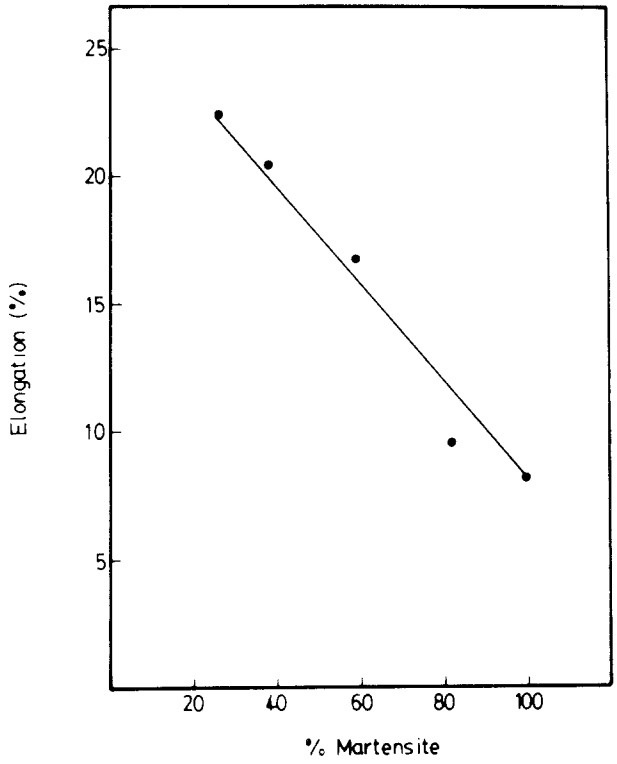

Figure 5 The variation of total elongation with the volume fraction of martensite.

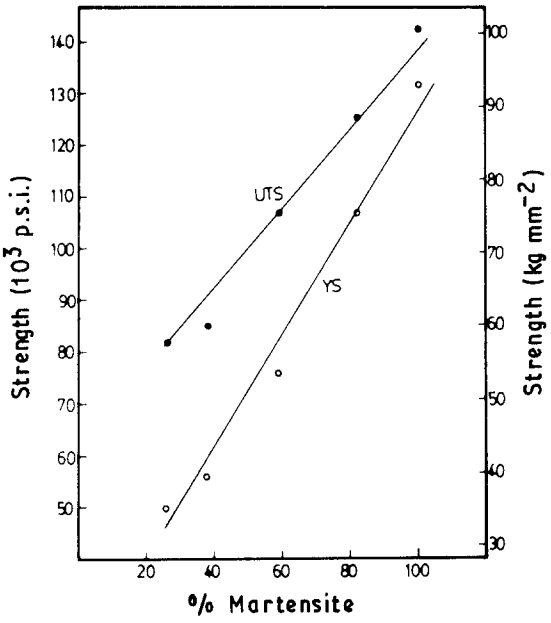

Figure 4 The variation of ultimate tensile and yield strengths with the volume fraction of martensite.

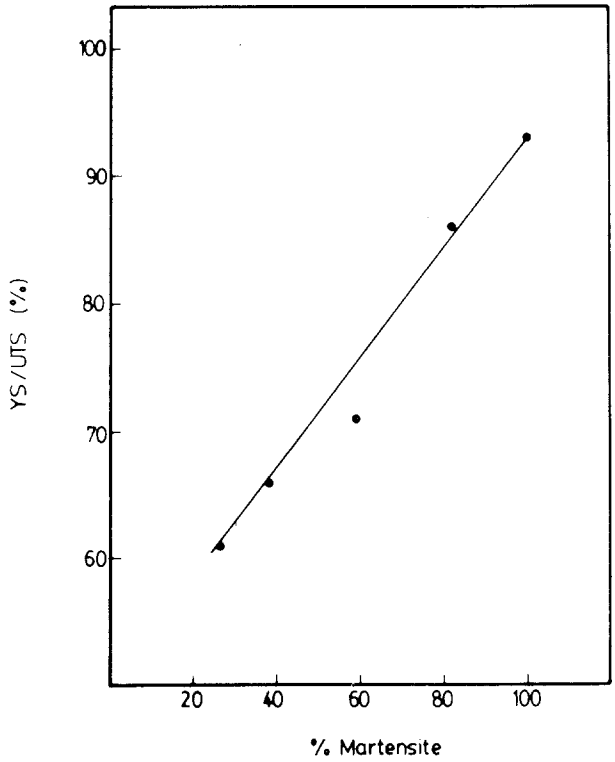

Figure 6 The variation of the YS/UTS ratio with the volume fraction of martensite.

Fig. 4 shows the variation of yield and ultimate tensile strengths of the steels as a function of martensite volume fraction. The general trend shown in the figure is that the composite strengths obey the linear

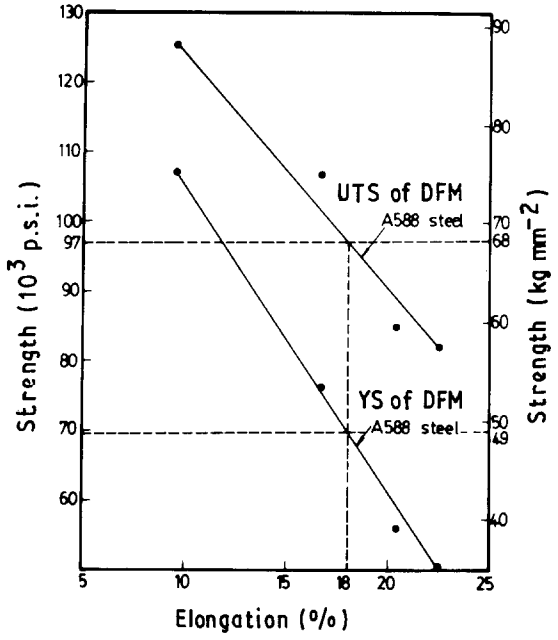

Figure 7 The variation of ultimate tensile and yield strengths with the total elongation for as-homogenized A588 steel. UTS = 48 kg mm^{-2}, YS = 30 kg mm^{-2}, elongation = 25.7%.

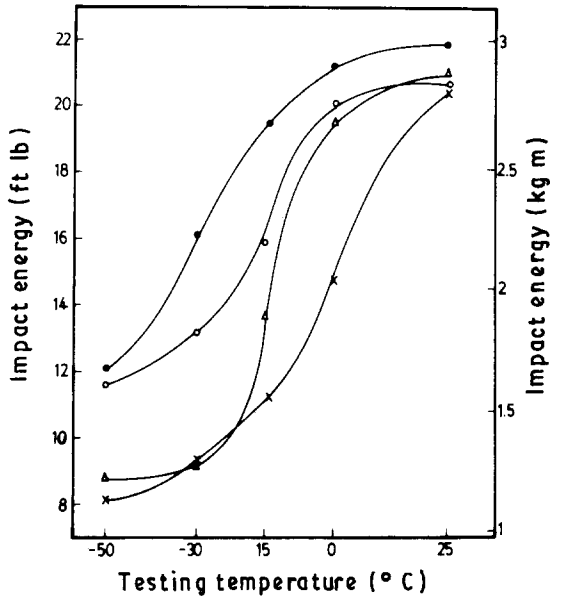

Figure 8 Charpy impact energy–testing temperature curves. Martensite content: (●) 82%, (○) 59%, (△) 38%, (×) 26%.

rule of two-phase mixtures. The variation of elongation with respect to martensite fraction is plotted in Fig. 5, demonstrating that the elongation decreases linearly with the volume fraction of martensite.

Fig. 6 shows the variation of YS/UTS as a function of volume fraction of martensite of the DFM steels. The curve also exhibits a linear relationship.

From these plots of strengths and elongation against fraction of martensite, it is evident that the dual-phase A588 steels possess a good combination of strength and elongation in the range 15% to 20% elongation. This is illustrated in a plot of strength against elongation as shown in Fig. 7. Note that for specimens with 18% elongation, UTS and YS are 68 kg mm^{-2} (97 × 10^3 p.s.i.) and 49 kg mm^{-2} (70 × 10^3 p.s.i.), respectively.

3.1.1.2. Impact properties. Charpy V-notch impact test was conducted at room temperature and subzero temperatures down to −50 °C to evaluate the room-temperature impact toughness of as-quenched DFM of A588 steel, to determine the influence of the fraction of martensite on the ductile to brittle transition temperature (DBTT), and to assess the DBTT characteristics of the DFM steel. The results of the impact study are presented graphically in Fig. 8. The data reported represent an average of at least three tests.

Fig. 8 shows the impact energy curves of as-quenched DFM of A588 steels with four different martensite volume fractions. The apparent transition temperature was lowered by increasing the martensite volume fraction. The DBTT of the curve with 26% martensite was determined to be about 0 °C, −13 °C for 38% martensite, −16 °C for 50% martensite, −30 °C for 82% martensite, correspondingly.

The impact energies of as-quenched DFM of A588 steels with four different martensite volume fraction at room temperature are more or less equal.

3.1.2. Optical metallography

The optical metallographs of DFM samples are shown in Figs 9 and 10. Fig. 9 shows the structure of samples annealed at 825 °C for various periods of time. For samples annealed at 825 °C for 5 sec, the microstructure must be tempered martensite as shown in Fig. 9a. Fig. 9b shows the grain-boundary patches and interlath regions of martensite in a tempered martensite matrix for samples annealed at the same temperature for 10 sec. It clearly indicates that during annealing in the ($\alpha + \gamma$) region, formation of austenite from the initial martensite structure begins at the prior austenite grain boundaries as well as at the martensite lath boundary. In a sample annealed at 825 °C for 1 min, a continuous network of globular martensite along the prior grain boundaries and acicular martensite within the prior austenite grain were observed, and size of globular martensite became very large as shown in Fig. 9c. After 30 min annealing, the microstructure (Fig. 9d) consists of continuous globular martensite along the prior austenite grain boundaries and acicular martensite along the interlath boundary with ferrite matrix. A higher volume fraction of martensite was found in samples annealed for a longer period. Fig. 10 shows the structures for samples annealed at 775 °C for 30 sec, 1, 5 and 30 min, accordingly. It is notable that the structure is also tempered martensite in samples annealed at 775 °C for 30 sec as shown in Fig. 10a. This implies that the time taken for initiation of austenite at 775 °C is larger than that at 825 °C. For samples annealed at lower temperature for 30 min, the fraction of globular martensite along the prior austenite grain boundaries became less if compared to higher temperature annealing as presented in Figs 9d and 10d.

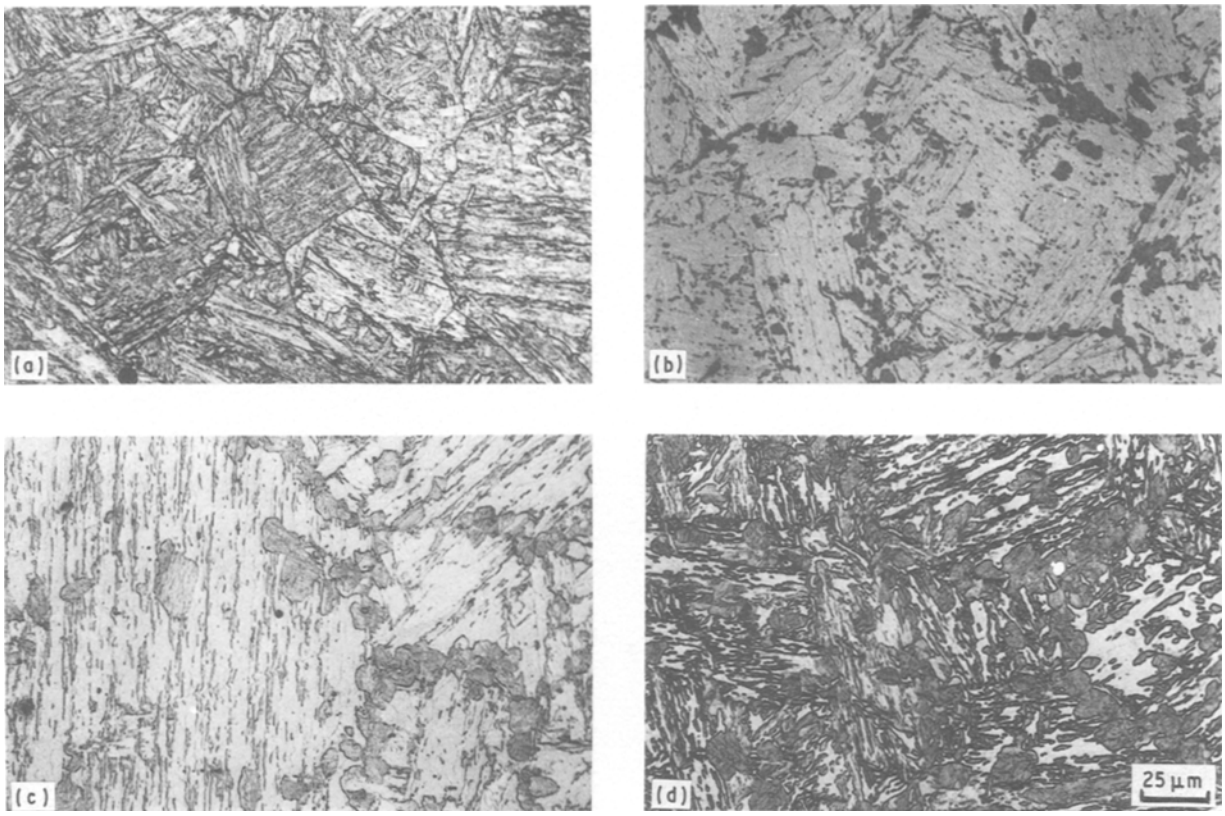

Figure 9 Optical micrographs of Q_2 treated specimens annealed at 825 °C for (a) 5 sec, (b) 10 sec, (c) 1 min and (d) 30 min (A30).

The annealing temperature in the ($\alpha + \gamma$) region determines not only the volume fraction of martensite but also the size of globular martensite particles.

3.1.3. Electron microscopy

For sample annealed in the ($\alpha + \gamma$) region, the initially homogeneously distributed carbon atoms in the martensite were segregated into carbon-enriched austenite (γ) leaving carbon depleted regions (α) behind. The proportion of each phase depends on the annealing temperature, if the equilibrium is reached. During quenching from the two-phase region, the austenite was transformed to martensite.

3.1.3.1. Morphology of martensite. The morphology of the martensite in A30 (82% martensite), B30 (59% martensite), and C30 (38% martensite) and D30 (26% martensite) was similar to the dislocated martensite structure, whereas the amount of twinning (microtwin) increased with a decreasing volume fraction of martensite for a given annealing time in the ($\alpha + \gamma$) region. The result is expected because the lower the volume fraction of martensite, the higher is the carbon content in the martensite, which can be easily seen from the iron–carbon phase diagram. Many microtwin areas were found in a D30 (26% martensite) specimen. They were internal microtwins embedded in the dislocated martensite. The martensites in A30 (82% martensite), B30 (59% martensite) and C30 (38% martensite) specimens are largely dislocated martensite. An example is shown in Fig. 11.

3.1.3.2. Morphology of ferrite. The retained ferrite was the matrix phase which did not undergo structural transformation after quenching from the ($\alpha + \gamma$) region to room temperature. During the annealing in the ($\alpha + \gamma$) region, the initial martensite structure was transformed to the ferrite and austenite. The ferrite formation can therefore be supposed to undergo the processes of recovery, recrystallization and grain growth in the initial martensite matrix. The result is a fine subgrain distribution in the ferrite areas. In addition, subsequent quenching from the two-phase region results in the generation of a high density of fresh dislocations in the ferrite region due to the accommodation strain caused by the austenite to martensite transformation. A representative example of the ferrite associated with fine grain size and high dislocation density is shown in Fig. 12. The ferrite grain sizes were about 1 to 3 μm.

3.2. Tempered DFM samples

The mechanical properties of tempered DFM steels with four different volume fractions are shown in Figs 13 to 16 for hardness, UTS, YS and elongation versus tempering temperatures, respectively. In Fig. 16, it is evident that the elongation decreases for 200 °C tempering and then increases up to 600 °C for all tempered DFM specimens except tempered A30 (82% martensite) which shows no evidence of decreasing up to 400 °C.

Fig. 17 is a micrograph of tempered B30 (59% martensite) at 200 °C. It is evident that the carbide precipitated at the lath martensite boundaries and within the

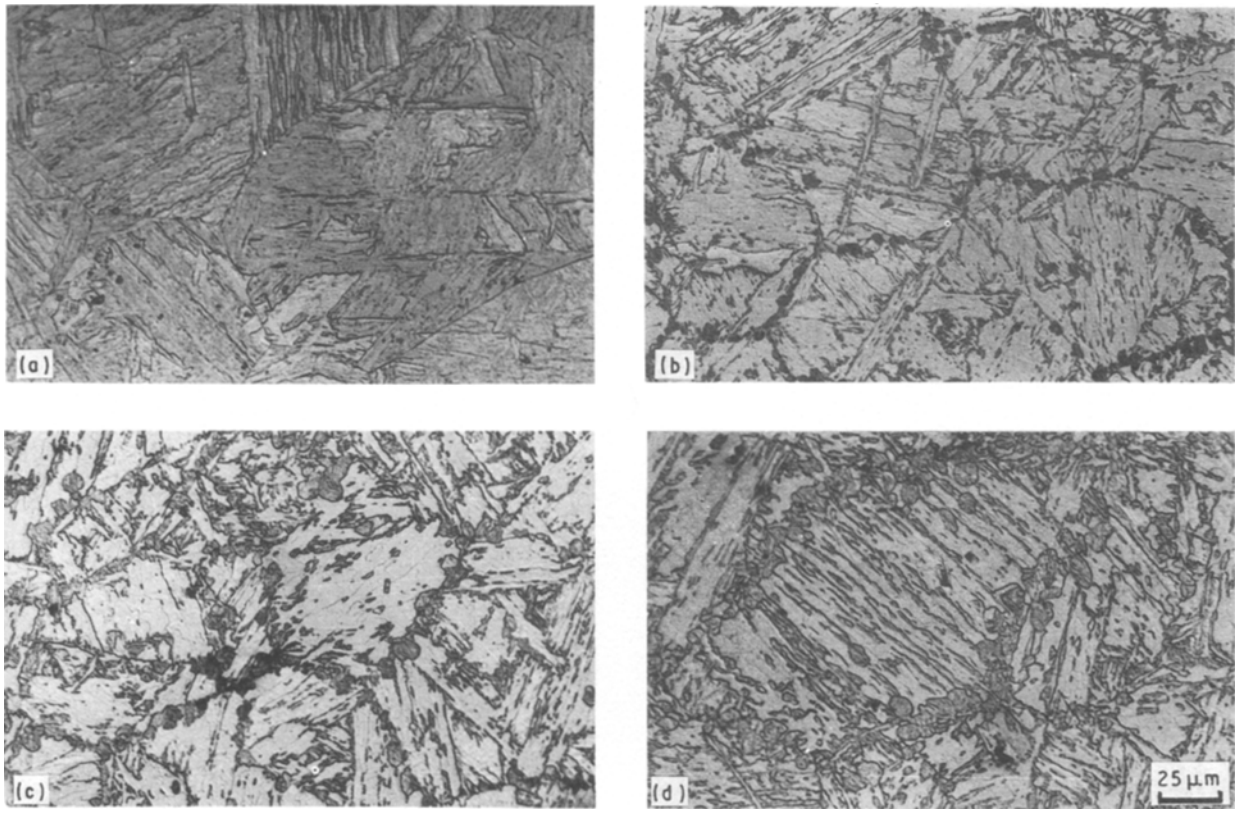

Figure 10 Optical micrographs of Q_2 treated specimens annealed at 775 °C for (a) 30 sec, (b) 1 min, (c) 5 min and (d) 30 min (C30).

Figure 11 B30 specimen with dislocated martensite.

Figure 12 C30 specimen, showing ferrite grains, 1 to 3 μm in size.

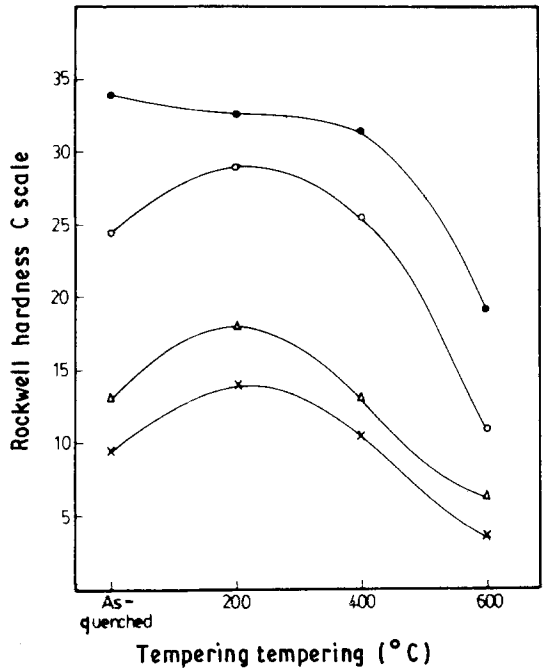

Figure 13 The variation of hardness of tempered DFM specimens with tempering temperature. For key, see Fig. 8.

lath martensite, which may explain why B30 tempered at 200 °C resulted in temper martensite embrittlement. For specimens tempered at 400 °C, the elongation was found to increase slightly. After tempering at 600 °C for 1 h, martensite regions were transformed to a completely recrystallized ferrite structure with irregularly spaced globules of cementite, while at ferrite regions, the dislocation density was further reduced. Fig. 18 shows the micrograph of C30 samples tempered at 600 °C. It can be seen that the coarsened and spheroidized carbides are located preferentially along the subgrain boundaries.

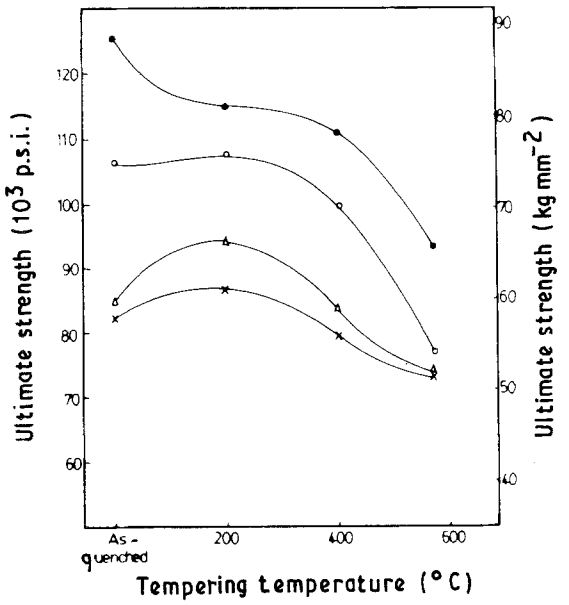

Figure 14 The variation of ultimate tensile strength of tempered DFM specimens with tempering temperature. For key, see Fig. 8.

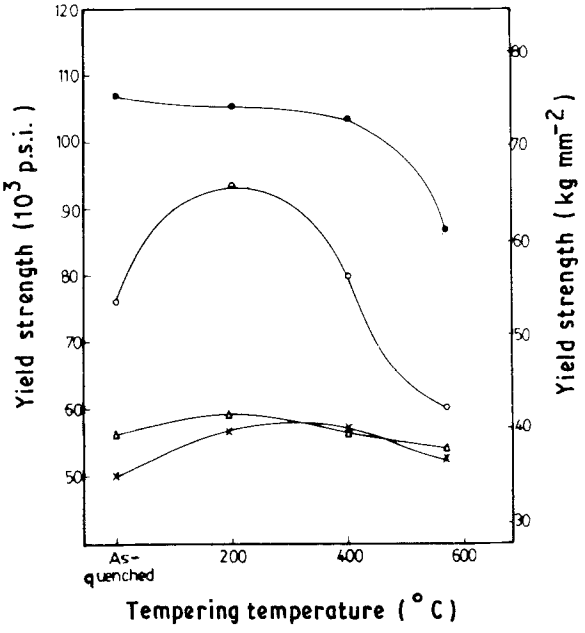

Figure 15 The variation of yield strength of tempered DFM specimens with tempering temperature. For key, see Fig. 8.

3.3. Variation of initial structures

To attain a controlled amount of martensite in a ferrite matrix, different heat treatments (Fig. 2), all of which involved phase transformation in the ($\alpha + \gamma$) region, were performed. A proper scheme of heat treatment will lead to specific morphology of DFM with desirable mechanical properties. It was intended to clarify the relationship between mechanical properties and DFM structures as well as the initial structures prior to subsequent annealing in the ($\alpha + \gamma$) region.

The variation of YS and UTS with elongation for different heat-treated samples are shown in Fig. 19. It is significant that Process I led to the best combination of strength and elongation, whereas Process III did not much improve the mechanical properties.

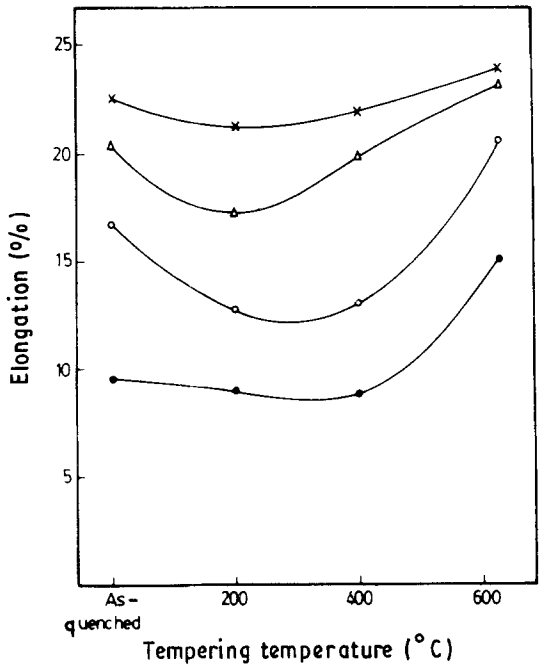

Figure 16 The variation of total elongation of tempered DFM specimens with tempering temperature. For key, see Fig. 8.

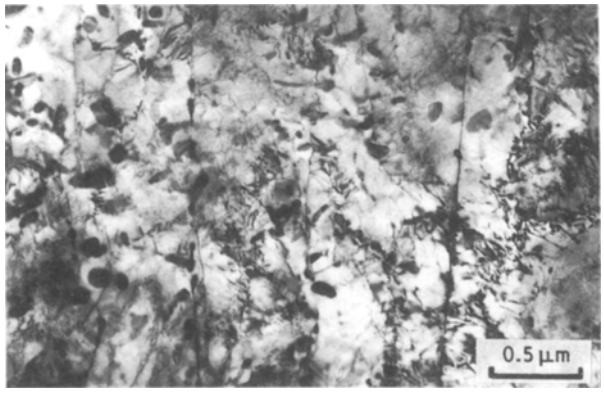

Figure 17 B30 specimen tempered at 200 °C showing the carbides precipitated at the lath boundary and in the lath martensite.

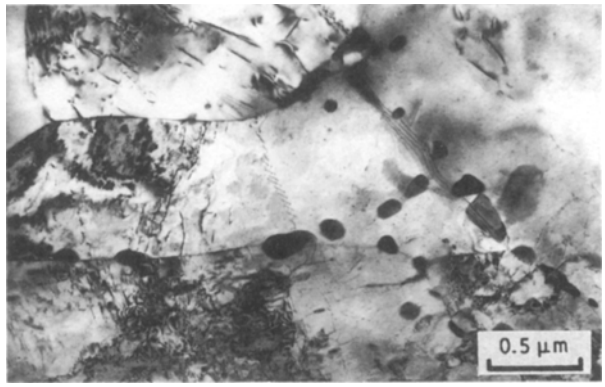

Figure 18 C30 specimen tempered at 600 °C, showing the coarsened and spheroidized carbides located preferentially along the subgrain boundaries.

The optical metallographs of different heat-treated samples are shown in Fig. 20. Fig. 20a (Process I) depicts the globular shape of martensite particles constituting a continuous network along the prior austenite grain boundaries and the acicular martensite

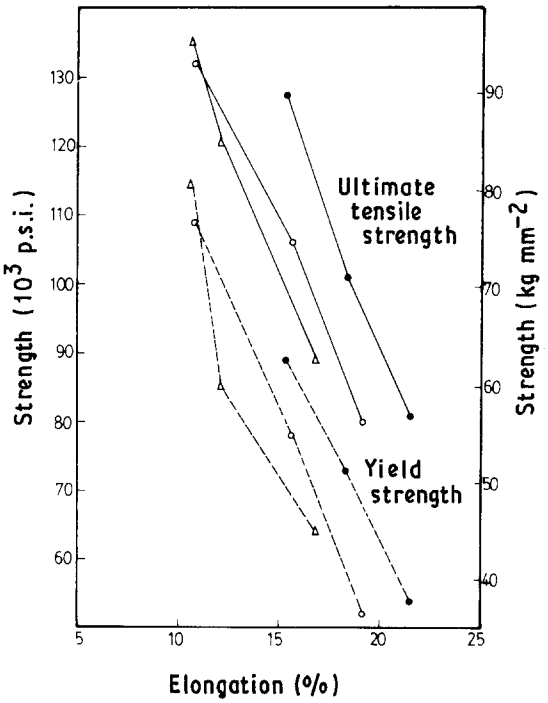

Figure 19 The strength–elongation curves for the specimens treated by Processes (●) I, (○) II, and (△) III.

particles within the prior austenite grains. Fig. 20b (Process II) shows that the ferrites are of irregular shapes mixed with martensites which lie mostly along prior austenite grain boundaries. Fig. 20c (Process III) illustrates that the ferrites are distributed along the prior austenite grain boundaries surrounding the martensites.

4. Discussion

4.1. The morphology of the DFM structure

The formation of austenite from martensite structure may occur by classical heterogeneous nucleations at such lattice imperfections as prior austenite grain, martensite lath boundary, matrix/carbide interface, etc. In the present study, the precipitation of austenite mainly occurred at prior austenite grain boundaries and martensite lath boundaries. At the same time, martensites undergo gradual transformation to ferrites and austenites for annealing in the ($\alpha + \gamma$) region. The dominating influence of the boundaries in the austenite nucleation process arises from the reduced activation energy for nucleation at the interfaces, as predicted by classical nucleation theory. However, some attention should be given to the role of substructural features of martensite in order to establish fully the mechanism that leads to the preferential nucleation in martensite structures. First of all, in the as-quenched martensite structure, the preference for the martensite lath boundaries as the austenite nucleation sites may be enhanced further by the presence of retained austenite along the lath boundaries, and the decomposition product of martensite such as carbides can also provide active sites for austenite nucleation.

The optical metallographs of A30, B30, C30 and D30 (e.g. see Figs 9d and 10d) show the globular shape of martensite particles constituting a continuous network along the prior austenite grain boundaries and the needle-like martensite particles in the prior austenite grains. For specimens annealed at higher temperature (e.g. A30) the size of globular martensite particles were larger and the amount of needle-like martensite particles was less. The morphology of a low-temperature annealed specimen (e.g. C30) was quite different from that of a high-temperature annealed specimen (e.g. A30). For C30 samples small but numerous globular martensite particles along prior austenite grain boundaries and large amounts of needle-like martensite particles were prominent. The higher the volume fraction martensite, the lower was the carbon content contained in the martensite, as can be seen from the iron–carbon phase diagram. Elements such as chromium and manganese easily segregate along the grain boundaries during solution treatment in the austenite region. When annealed in the ($\alpha + \gamma$) region, austenite nucleation at the prior austenite grain boundaries will be enhanced by the attractive interaction [11] between carbon and the chromium and manganese atoms already present at the boundaries if the annealing temperature is high. In addition, the growth rate of austenite is higher, not only due to the higher diffusion rate but also because of requiring a lower carbon content at the front of the interface for transformation to occur at higher temperature. This may be the reason why larger globular martensite particles were obtained at higher annealing temperatures.

4.2. Mechanical properties of duplex A588 steel

4.2.1. Tensile properties

Fig. 4 shows the variation of yield and ultimate strengths of the dual-phase treated steel as functions of martensite volume fraction. The general trend shown in the figure is that the composite strengths obey the linear rule of two-phase mixtures. The data of Koo and Thomas [4, 12, 13], Tamura *et al.* [14], Hayami and Furukawa [8] and Davies [6] for plain carbon steels and alloy steels, suggested that the strength of dual-phase alloys arises from the mechanical mixture of soft ferrite and strong martensite, in spite of the absence of an exact theoretical explanation.

Yield strength and ultimate strength are functions of the percentage of martensite in the DFM steels and do not depend upon the carbon content of the martensite. The major question raised by the strength results is why the high-carbon martensite structures have the same apparent strength as the low-carbon martensite structures.

Two of the factors [6] that could be contributing to the lowering of the yield strength of high-carbon martensite structure are: (i) the large transformation strains in retained austenite, and (ii) a larger Bauschinger effect [15] due to the lower transformation temperature and larger transformation strains in the higher carbon martensite.

It has also been suggested [6] that the factors contributing to the lowering of the ultimate strength of high-carbon martensite structure in the dual phase at

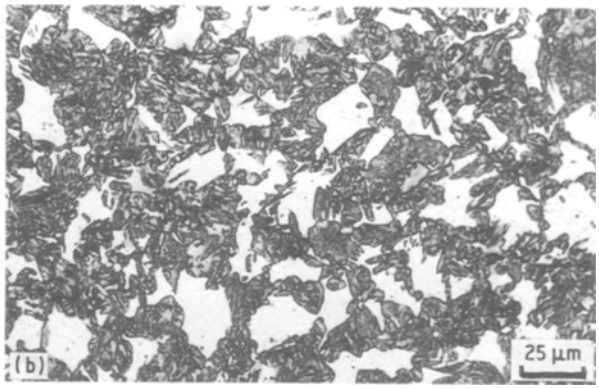

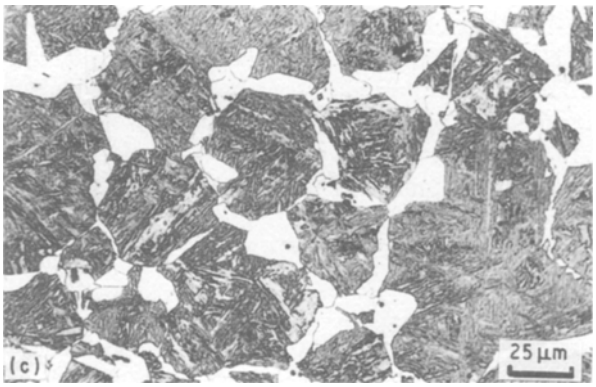

Figure 20 Optical micrograph showing DFM structures obtained by (a) Process I, (b) Process II, and (c) Process III treatments.

high strains are: (i) martensite cracking which usually occurred when the carbon content was high, and (ii) the higher carbon content leading to the proliferation of twinned martensite which has poor toughness. High-carbon martensite will rupture rapidly at high strains.

From Fig. 7, it is noted that the dual-phase steel possesses a good combination of strength and elongation in the range 15% to 20% elongation, especially for the sample with 18% elongation, a UTS value of 68 kg mm^{-2} (97 × 10^3 p.s.i.) and YS of 49 kg mm^{-2} (70 × 10^3 p.s.i.).

4.2.2. Impact properties of the DFM steel

The impact properties of DFM steels are strongly affected by three major structural factors: morphology (shape, size and distribution) of DFM structure, volume fraction of martensite particles, and toughness (carbon content) of the martensite particles. As the volume fraction of martensite decreases it is expected that (1) the connectivity of martensite will decrease, thus resulting in better impact properties, and (2) the carbon content in the martensite will increase, and therefore the toughness, and thus impact properties, of martensite will deteriorate. The carbon level has a drastic effect on reducing the notched impact energy and increasing the ductile to brittle transition temperature (DBTT) [16]. Fig. 8 shows the impact energy curves of DFM steel with four different martensite volume fractions. The energy curve with higher volume fraction (82% martensite) corresponds to better impact properties and the lower DBTT ($\sim -30\,^\circ$C), while DBTT was 0 °C for the curve with the lower volume fraction (26% martensite). This result may be due to the fact that the toughness factor exerts more influence than the connectivity factor.

4.3. Tempering behaviour of DFM steels

For DFM samples tempered at 200 °C for 1 h, appreciable amounts of carbides were precipitated in the martensite and at the lath boundaries, as shown in Fig. 17. It is evident that the carbides were mainly in the form of interlath films and globular particles. The interlath films of carbides may be due to the decomposition of retained austenite [17]. These carbides may perhaps induce an embrittlement at 200 °C. Upon tempering, most low-alloy steels exhibit a temper martensite embrittlement at low-temperature tempering [18]. Temper martensite embrittlement may occur as a result of retained austenite decomposition at the lath boundaries to form cementite, and manganese and chromium promote the decomposition of austenite at a lower temperature [18], which may explain why temper martensite embrittlement for DFM occurred around 200 °C tempering.

On tempering at 400 °C for 1 h, the martensite structures were mostly decomposed, and elongation of the specimen gradually increased. After tempering at 600 °C for 1 h, the martensite regions were transformed to a completely recrystallized ferrite structure with irregularly spaced globules of cementite, while the dislocation density in ferrite regions was further reduced. In Fig. 18, it can be seen that the coarsened and spheroidized carbides are located preferentially along the recrystallized subgrain boundaries. This may be due to excess carbon draining from the ferrite to form carbides in the prior martensite regions and starting to coarsen.

4.4. Variation of initial structures

The initial structure of Process I prior to subsequent annealing in the ($\alpha + \gamma$) region was 100% martensite as shown in Fig. 2. In Processes II and III, the initial structures were fine pearlite plus proeutectoid ferrite, and austenite, respectively.

It is evident that the initial martensite structure has several advantages: i.e. (i) it provides sufficient heterogeneous nucleation sites for austenite at prior austenite grain boundaries during two-phase annealing,

and (ii) parallel laths of very narrow width within a prior austenite grain can produce a fine fibrous distribution of acicular martensite in a ferrite matrix, as depicted in Fig. 20a. From the results of mechanical testing (see Fig. 19), it is apparent that the initial martensite structure is more beneficial in obtaining a suitable DFM morphology with a good combination of strength and ductility.

5. Conclusions

An investigation was made on DFM treatments of ASTM A588 steel. Based on the study of duplex microstructure–property relationships, the following conclusions were drawn.

1. The type of initial microstructure prior to dual-phase treatment is of prime importance in the determination of the morphology of DFM structures, because upon reheating to the two-phase region, the nucleation and growth of austenite from the initial structure is strongly influenced by their microstructural details.

2. The initial martensite structure prior to subsequent annealing in the $(\alpha + \gamma)$ region offers several advantages: (i) it provides sufficient heterogeneous nucleation sites for austenite at prior austenite grain boundaries during two-phase annealing, and (ii) parallel laths of very narrow width within a prior austenite grain can be utilized to produce a fine, fibrous distribution of acicular martensite in a ferrite matrix.

3. The initial martensite structure of the steel annealed in $(\alpha + \gamma)$ region may be used to produce a DFM structure with continuous globular martensite along the prior austenite grain boundaries and acicular martensite within prior austenite grains. The continuous globular martensite along the prior austenite grain boundary, as an inevitable product of the phase transformations in the system, is detrimental to mechanical properties.

4. The morphology of DFM steel was affected by annealing temperature for a given annealing time. For samples annealed at higher annealing temperature, a large fraction of bulky continuous globular martensite and a small amount of acicular martensite were formed. For annealing at lower temperature, more acicular martensite and small-sized globular martensite were observed.

5. Over the range 20% to 80% martensite, the linear rule for two-phase mixtures appears to hold as a good approximation of the tensile behaviour of the duplex system.

6. DFM of the steel exhibits a superb combination of strength and elongation over a range of elongation 15% to 20%. For a sample with 18% elongation, YS = 49 kg mm^{-2} (70×10^3 p.s.i.) and UTS = 68 kg mm^{-2} (97×10^3 p.s.i.).

7. Impact properties are strongly influenced by the connectivity, carbon concentration, and volume fraction of martensite. A less connected, low-carbon concentration and high volume fraction of martensite are desired.

8. Tempering at 200 °C for 1 h resulted in the temper martensite embrittlement. This may be due to carbide precipitation as the result of decomposition of the retained austenite.

9. Alloy elements chromium and manganese in the steel may easily segregate to the prior austenite grain boundary. It promotes carbon diffusion and the formation of globular martensite at the prior austenite grain boundary which make the successful design of a full fibrous morphology of DFM for the A588 steel difficult.

References

1. H. C. CHEN and G. H. CHENG, *J. Mater. Sci.* **24** (1989) 1991.
2. A. NAKAGAWA, J. Y. KOO and G. THOMAS, *Met. Trans.* **12A** (1981) 1965.
3. A. R. MARDER, *ibid.* **12A** (1981) 1569.
4. J. Y. KOO and G. THOMAS, *ibid.* **8A** (1977) 525.
5. R. G. DAVIES, *ibid.* **9A** (1978) 41.
6. *Idem, ibid.* **9A** (1978) 671.
7. L. J. RAMOS, D. K. MATLOCK and G. KRAUSS, *ibid.* **10A** (1979) 29.
8. S. HAYAMI and T. FURUKAWA, in "Micro Alloying 75", edited by J. Crane (Union Carbide Corporation, New York, 1977) p. 311.
9. H. E. McGANNON (ed.), "The Making, Shaping and Treating of Steel" (US Steel Company, 1971) p. 1148.
10. E. C. BAIN and H. W. PAXTON, "Alloying Elements in Steel", 2nd Edn (ASM, Metals Park, Ohio, 1961) p. 104.
11. *Idem, ibid.*, p. 243.
12. J. Y. KOO and G. THOMAS, *Mater. Sci. Engng* **24** (1976) 187.
13. J. Y. KOO, PhD thesis, University of California, Berkeley (1977).
14. I. TAMURA, Y. TOMOTA, A. AKAO, Y. YAMCOKA, M. OZAWA and S. KANATANI, *Trans. Iron Steel Inst. Jpn* **13** (1973) 283.
15. R. W. K. HONEYCOMBE, "The Plastic Deformation of Metals" (St. Martin's Press, New York, 1968) p. 401.
16. R. R. PRESTON, *J. Metals* **29** (1977) 9.
17. R. M. HORN and R. O. RITCHIE, *Met. Trans.* **9A** (1978) 1039.
18. G. THOMAS, Met. Trans. **9A** (1978) 439.

Received 16 October 1989
and accepted March 1990